Journal of GeoEngineering, Vol. 18, No. 4, pp. 183-193, December 2023
http://dx.doi.org/10.6310/jog.202312_18(4).2

INVESTIGATION OF MECHANICAL BEHAVIORS OF A NEAR-SLOPE TILTED-SEAM MINING EXTRACTION USING DISCONTINUOUS DEFORMATION ANALYSIS

Trong Nhan Do [1] and Jian-Hong Wu [2*]

ABSTRACT

Clarifying mechanical behaviors of a rock slope during coal-mining extraction is a challenging task because the mining operation causes serious surface subsidence and stress changes, which may result in a chain reaction of a landslide. A tilted-seam extraction in a jointed rock cliff induced a massive landslide at Nattai North of Australia is investigated using Discontinuous Deformation Analysis (DDA). A small-scale model of the coal-mining operation is simulated by a physical trap-door model and the numerical DDA. Comparisons of actual surface ground subsidence and stress result from the DDA and the trap-door experiment, whose geometry is similar to that of the Nattai North coal mine, verify the correctness of the DDA simulations. Next, the mechanical behavior of the rock mass prior to the initiation of the slope failure in Nattai North of Australia is investigated by the DDA. The computational results of subsequent DDA simulation of the inclined-seam mining extraction at the coal mine show that the near-vertical joints govern the subsidence pattern. The rocks above the mining seam significantly sink, which causes serious subsidence at the ground surface. High-stress concentration around mined zone results in fractures of rock blocks near the toe of the slope, which is a key reason to cause a subsequent landslide.

Key words: Discontinuous Deformation Analysis (DDA), physical trap-door model, surface subsidence, high-stress concentration, jointed rock mass, tilted-seam extraction.

1. INTRODUCTION

Many mineral resources have been widely mined to meet the demands of unstoppable industrial development, especially coal mining for energy consumption, which causes serious mining subsidence across the globe (Dunrud and Osterwald 1980; Pells *et al.* 1987; Singh and Yadav 1995; Holla 1997; Choi *et al.* 2010; Sasaoka *et al.* 2015; Zheng *et al.* 2019). Mining-induced ground subsidence significantly damages not only superstructures on the ground, such as for public transportation and habitation (Aleshina *et al.* 2008; Song *et al.* 2012), but also natural environments, for example, agricultural land (Jing *et al.* 2018; Bi *et al.* 2019), artesian-water sources (Dai *et al.* 2011; Chen *et al.* 2019)), and even human lives (Yang and Ho 2019). Additionally, underground-seam extraction has been known to cause flooding, such as in the middle of the 19th century in the Ruhr district of Germany (Bell *et al.* 2000); surface cavities collapse and ruptured casing or other buildings damage near Gardanne, France (Carnec and Delacourt 2000); and sinkholes and landslides in the Ebro River valley in Zaragoza, Spain (Castañeda *et al.* 2009). Therefore, consolidating the knowledge of the mechanism of mining-induced ground deformation is extremely essential to find practical solutions for mitigating ground damage and increasing safety for human lives.

Full-scale experiments (Ghabraie *et al.* 2015), empirical prediction methods (Britain 1966), and numerical simulation methods (Vyazmensky *et al.* 2007; Do and Wu 2020a; Do and Wu 2020b) are available approaches to clarify the mechanical behavior of the ground during mining operations. Full-scale models are not practical because of their high cost and the difficulty in reproducing the experiments (Meguid *et al.* 2008). Empirical methods are easy to understand but cannot fully consider different site-dependent characteristics (Ambrožič and Turk 2003). In contrast, numerical simulation methods have been widely applied to study ground deformation during mining extraction with overwhelming advantages considering geometry, natural-material properties, and complicated topography (Najjar and Zaman 1993; Xu *et al.* 2013). Among such simulation methods, the Distinct Element Method (DEM) (Wu and Hsieh 2021a, 2021b) and Discontinuous Deformation Analysis (DDA) (Chen *et al.* 2010) are widely used to address issues in rock mechanics involving discontinuities. In contrast to the DEM, DDA is an implicit approach, so its global matrix converges more easily (Jing *et al.* 2001; Wu 2010). Many researchers have successfully simulated excavation-induced ground-deformation problems in jointed rock masses to verify the use of DDA in underground constructions (Wu *et al.* 2004; Zhu *et al.* 2016; Do *et al.* 2017; Wu *et al.* 2018).

However, simulating different case studies to clarify individual failure mechanisms involving complicated geometry is essential to assess the practical application of numerical simulations. Clarifying the rock-mass failure mechanism at the coal mine in Nattai North of Australia is a challenging task because the mining was conducted in a jointed rock mass by tilted-seam extraction that eventually induced a landslide (Fathi Salmi *et al.* 2017). Therefore, this study investigates the mechanical behavior of the rock mass at the mine prior to the landslide. In the beginning, a small-scale model of the study site is reproduced by a physical trap-door

Manuscript received May 10, 2023; revised August 14, 2023; accepted August 30, 2023.
[1] Assistant Professor, Department of Transportation Engineering, Can Tho University, Viet Nam.
[2*] Professor (corresponding author), Department of Civil Engineering, National Cheng Kung University, Tainan, Taiwan (e-mail: jhwu@mail.ncku. edu.tw).

model and DDA numerical simulation. Surface subsidence and stress distribution results calculated from DDA simulation are confirmed by experimental results measured from the trap-door model. Finally, DDA is employed to investigate the kinematic behavior of the rock mass at Nattai North landslide.

2. STUDY SITE

The coal mine at Nattai North, Australia, approximately 80 km southwest of Sydney, is a well-known mining-induced-landslide case-study site (Fig. 1). The total rock-mass failure amounted to approximately 30 million tons from 1965 to 1984 (Cunningham 1988). The breakdown of the escarpment can be divided into two stages. In 1965, the rock cliff experienced the first collapse, which caused 3 million tons of rock-mass failure followed by many small rockfalls. More notably, the significant collapse of the cliff happened five years later. From the middle to the late 1970s, approximately 25 million tons of rock mass detached from the escarpment and reached the shore of Lake Burragorang (Fig. 1). The total volume of debris was approximately 14 million cubic meters, and the height was 200-300 m (Fathi Salmi *et al.* 2017). At that time, the landslide was considered one of the largest rockfall avalanches in Australia (Mostyn *et al.* 1997).

Previous researchers have discussed the characteristics of the topography and the mining operation of the case study (Pells *et al.* 1987; Mostyn *et al.* 1997; Keilich *et al.* 2006; Fathi Salmi *et al.* 2017). Figure 2 shows the cross-section A-A' (Fig. 1) of the escarpment which is modified from (Pells *et al.* 1987). The bedding planes incline into the slope with an angle of 5°, and the subvertical joints dip out of the slope at 84°. The weak and easily fractured Wombarra Claystone is overlain by two competent rock layers, the Scarborough Sandstone and Bulgo Sandstone, which therefore subject the thinner claystone layer to very high stress (Fig. 2). In the late 1950s, well before the first landslide occurred in 1965, inclined-seam coal mining was started beneath the slope toe. The working direction of the mining was headed towards the cliff face. The mining-induced subsidence and change in shear stress near the slope toe have been considered the main triggers for the subsequent landslide (Cunningham 1988; Mostyn *et al.* 1997).

Fathi Salmi *et al.* (2017) firstly investigated the failure mechanism of the study site using a distinct element method software, called UDEC, and concluded that the joint displacement near the ming area plays an important role on the failure mechanism of the site. Because the block in the study of Fathi Salmi *et al.* (2017) is assumed to be rigid with distinct element method, stress distributions of the rocks and the relationship between the failure process of the landslide and the joint displacement remained unclear. Because DDA has advantages of elastic blocks and large block displacement, the major objective of our study is to use DDA to produce numerical evidence to clarify the kinematic behavior resulting from coal mining at Nattai North of Australia and determine possible causes of the landslide.

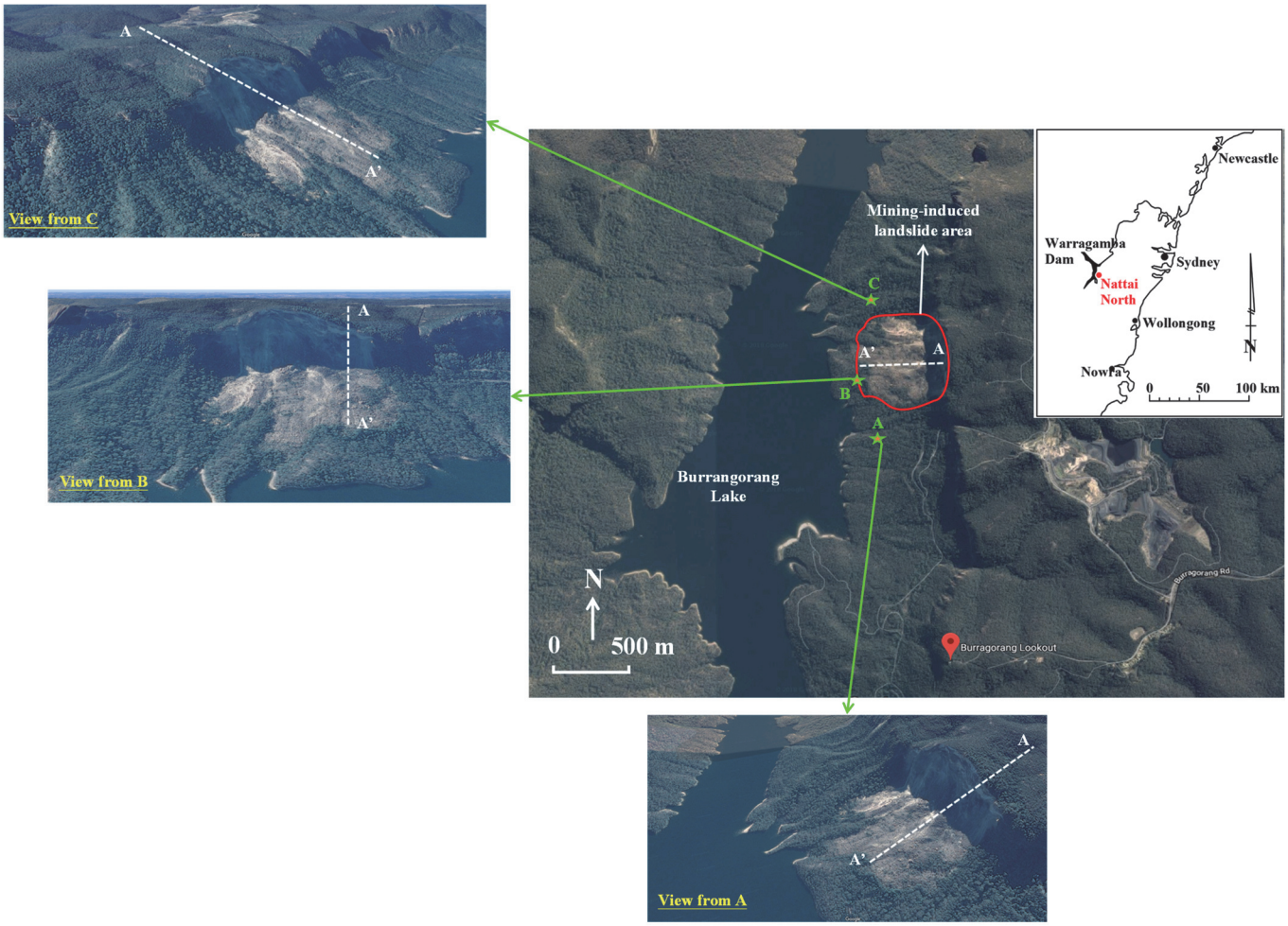

Fig. 1 Location of the case study (The satellite images come from Google Earth)

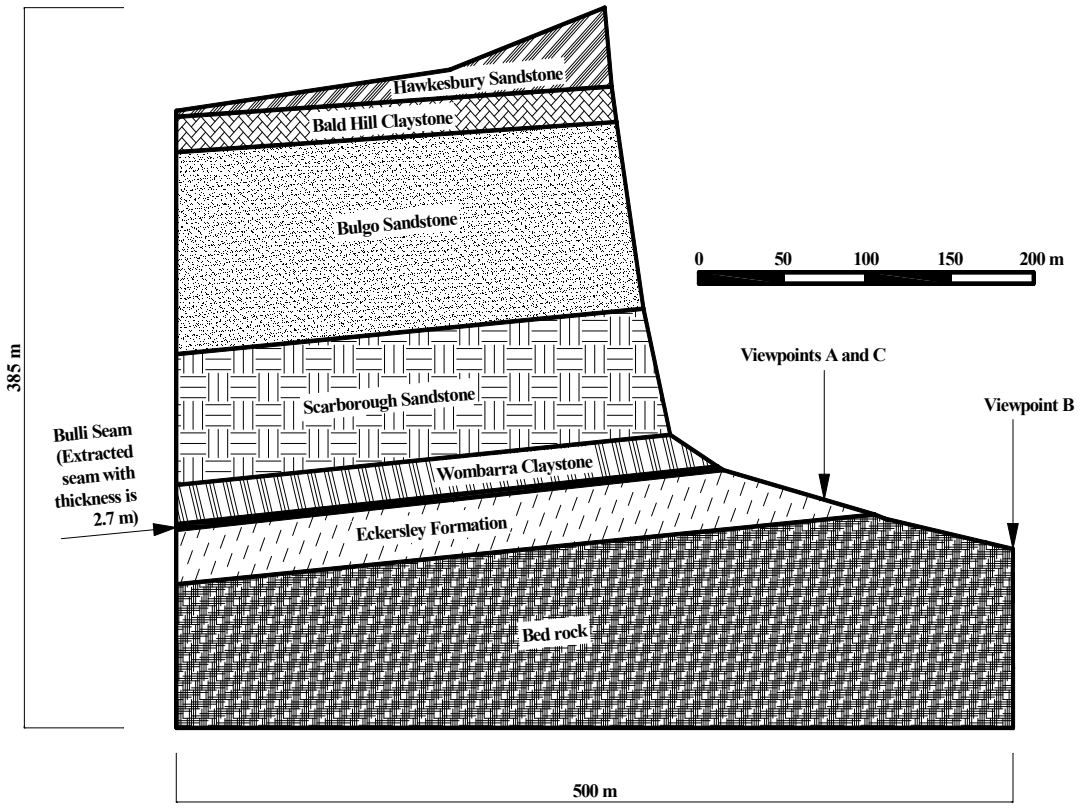

Fig. 2 The cross-section A-A' of the escarpment modified from Pells *et al.* (1987)

3. DISCONTINUOUS DEFORMATION ANALYSIS (DDA)

The DDA discovered by Shi (1989) is a discrete element method, which allows simulating the behavior of a blocky rock mass with large displacement. In two-dimensional DDA version, the behavior of arbitrary point (x, y) within a block can be described by six unknown variables (u_0, v_0, r_0, ε_x, ε_y, γ_{xy}) and the displacement (u, v) of the point (x, y) can approximate to the linear displacement function in Eq. (1) with the assumption of constant stress and strain in an individual elastic and unbreakable block.

$$\begin{Bmatrix} u \\ v \end{Bmatrix} = \begin{bmatrix} 1 & 0 & -(y-y_0) & (x-x_0) & 0 & \dfrac{(y-y_0)}{2} \\ 0 & 1 & (x-x_0) & 0 & (y-y_0) & \dfrac{(x-x_0)}{2} \end{bmatrix} \begin{Bmatrix} u_0 \\ v_0 \\ r_0 \\ \varepsilon_x \\ \varepsilon_y \\ \gamma_{xy} \end{Bmatrix} = [T_i].\{D_i\} \quad (1)$$

where (u_0, v_0) is the rigid-body translational displacement around the centroid (x_0, y_0) of the block, r_0 is the rigid-body rotation around the centroid (x_0, y_0), and ε_x, ε_y, γ_{xy} are normal- and shear-strain components.

The block system is an assembly of many blocks (n-block). Arbitrarily, two blocks are in mutual edge-to-edge, vertex-to-vertex, or vertex-to-edge contact (Fig. 3(a)). When two blocks contact each other, the spring stiffness under normal (k_n) and shear (k_s) contact govern the penetrating, sliding, and separating motions between the blocks (Fig. 3(b)). Minimizing the total potential energy in an n-block system, such as from the initial constant stress, the volume force, the points loading, the contact forces, the constraint spring of the fixed points, and so on, results in the following global matrix (Eq. (2)). The equation can be solved with the requirements of non-tension and non-penetration among the blocks.

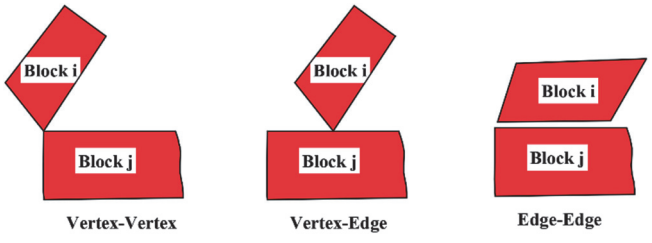

(a) Three kinds of contact in DDA

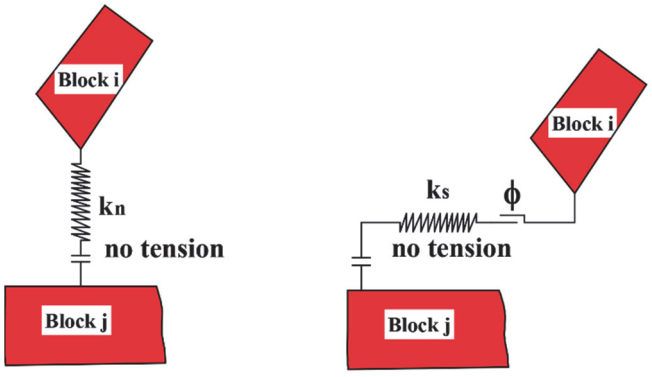

(b) Virtual springs in DDA when two blocks contact

Fig. 3 Contact in DDA simulation

$$\begin{pmatrix} K_{11} & K_{12} & K_{13} & \dots & K_{1n} \\ K_{21} & K_{22} & K_{23} & \dots & K_{2n} \\ K_{31} & K_{32} & K_{33} & \dots & K_{3n} \\ \dots & \dots & \dots & \dots & \dots \\ K_{n1} & K_{n2} & K_{n3} & \dots & K_{nn} \end{pmatrix} \begin{pmatrix} D_1 \\ D_2 \\ D_3 \\ \dots \\ D_n \end{pmatrix} = \begin{pmatrix} F_1 \\ F_2 \\ F_3 \\ \dots \\ F_n \end{pmatrix} \quad (2)$$

where D_i (i, j = 1, 2, $\cdots$, n) is the 6 × 1 submatrix of the deformation variables, F_i (i, j = 1, 2, $\cdots$, n) is the 6 × 1 submatrix of the loading, and K_{ij} (i, j = 1, 2, $\cdots$, n) is the 6 × 6 submatrix of the contacts between blocks i and j.

4. PHYSICAL TRAP-DOOR MODEL

The physical trap-door model is an effective and flexible tool to model underground excavations with different types of geomaterials, including sand (Tanaka and Sakai 1993), gravel (Thongprapha *et al.* 2015), and jointed rock mass modeled by aluminum blocks (Do *et al.* 2017) for different topographies (Park and Adachi 2002). In addition, the experimental results can be used as references to verify the correctness of the numerical-simulation program results.

The trap-door model is 800 mm in height, 300 mm in length, and 200 mm in width (Fig. 4(a)). The rotary control jack and the bearing steel bar on the right side are devices to manually rotate the whole trap-door model. A laser displacement sensor attached to the driving shafts measures the ground movements during mining extraction, which is performed by lowering the trap-door panel an assigned amount. Governed by the speed control box, the laser displacement sensor is moved along the drive shafts by the electric motor. Thirteen load cells replace the supporting blocks (at the bottom of the rods below the aluminum blocks) (Fig. 4(a)) to measure the change of loadings at different locations before and after lowering the trap-door panel.

Figures 4(b) and 4(c) show the accessories used in the trap-door model, the laser displacement sensor, the load cell, and the dimensions of the aluminum blocks and rods. The jointed rock mass is modeled by the aluminum blocks and rods. The width of the trap-door panel is D = 100 mm. Park (2001) and Park and Adachi (2002) suggested introduce aluminum rods to the lower boundary of the aluminum blocks to prevent the loads along the bottom from transferring irregularly through the contact between blocks.

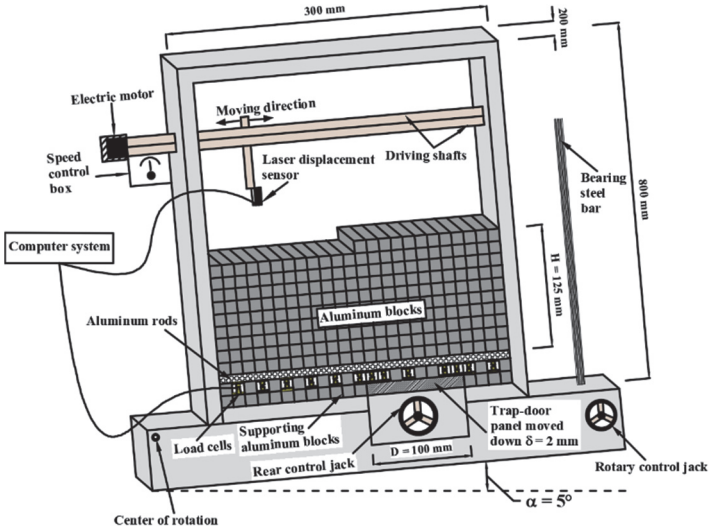

(a) Trap-door model

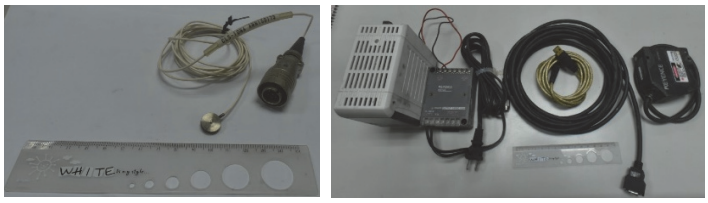

(b) Laser displacement sensor (left photo) and load cell (right photo)

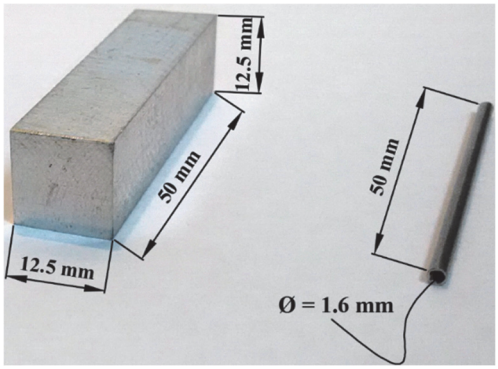

(c) Aluminum block and rod

Fig. 4 The small-scale model of the study site in the trap-door model and accessories for the experimental test

5. SMALL-SCALE MODEL OF THE STUDY SITE

5.1 The Small-scale of the Study Site in the Trap-door Model

The simulated-mining process of the study site in the trap-door test includes the following steps:

Step 1: To demonstrate mining in mountainous terrain, the deposited aluminum blocks and rods (Fig. 4(c)) are arranged as shown in Fig. 4(a). The height of the deposited aluminum block is H = 125 mm. Then, the trap-door model is rotated counterclockwise around the center of rotation at α = 5° from the horizon (Fig. 4(a)), which models the dip angle of the bedding planes in the study site (Nattai North, Australia). The amount of lowering of the trap-door panel represents the thickness of the mining seam, set at δ = 2 mm.

Step 2: The laser displacement sensor (Fig. 4(b) with left photo) is installed to detect the initial coordinates of the surface blocks, and the load cells (Fig. 4(b) with right photo) are used to measure the initial earth loadings.

Step 3: Lowering the trap-door panel at δ = 2 mm by the rear control jack at the bottom (Fig. 4(a)) simulates the mining extraction process. Gravity forces the deposited aluminum blocks and rods to slide and fall, which causes the ground subsidence. The laser displacement sensor detects the coordinates of the surface blocks, and the load cells measure the earth loading after mining excavation.

Step 4: The surface subsidence is the difference of the coordinates of the surface blocks between Steps 3 and 2. To determine the earth-pressure normalization, the earth loadings from Step 3 are divided by the values from Step 2.

Step 5: The surface-subsidence profile and the earth-pressure normalization curve are plotted.

5.2 The Small-scale Model of the Study Site in DDA Simulation

Figure 5 shows the simplified geometric model of the small scale of the study site in the DDA simulation, which corresponds to that in the trap-door test in Fig. 4(a). The width of the trap-door panel is D = 100 mm, and the height of the deposited aluminum blocks is H = 125 mm. A small gap between the trap-door panel and the bottom layer of the deposited aluminum blocks represents the amount of lowering of the trap-door panel (δ = 2 mm) in the experimental test. Additionally, the numerical model is tilted at an angle of α = 5° to the horizon, as in the trap-door model in Fig. 4(a). At the two sides of the trap-door model, the supporting aluminum blocks and the trap-door panel are considered to be fixed in the DDA (Fig. 5). The aluminum rods in Fig. 4(a) are simplified as frictionless joints in DDA model to simulate the motion of the aluminum rods in the trap-door model because the DDA software used in this study cannot simulate circular blocks and too many rod blocks result in very expansive computation costs. Tables 1 shows the physical properties of the aluminum blocks and Table 2 is the numerical parameters used in the DDA simulation (Do *et al.* 2017). The soft contact spring with stiffness of 380 kN/m is obtained by trial and error, and the dynamic control parameter is set to be 0.99 to accelerate the convergence of simulating the pseudo-static problem of the trap-door test after the suggestion from Wu *et al.* (2004).

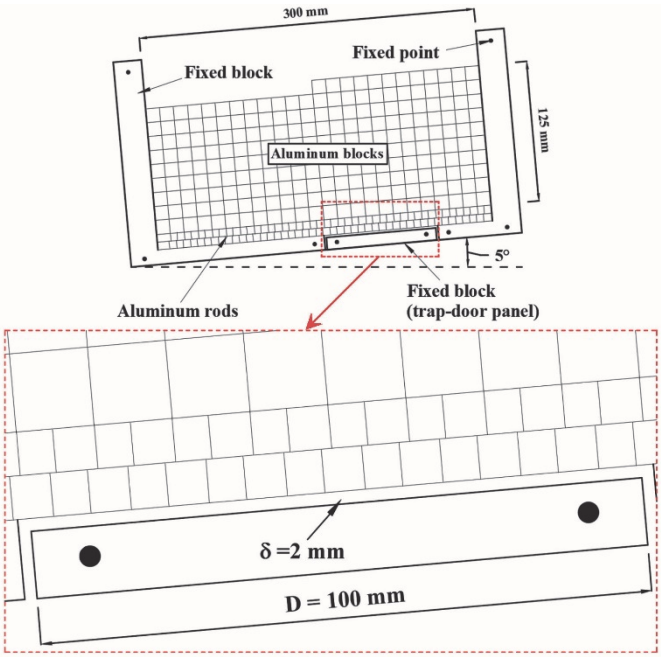

Fig. 5 The small-scale model of the study site in DDA simulation

Table 1 Physical properties of the aluminum blocks

Physical properties of aluminum blocks		Values
Joint	Friction angle (°)	22.0
	Cohesion (kPa)	0.0
	Tensile strength (kPa)	0.0
Block	Density (g/cm^3)	2.7
	Unit weight of rock (kN/m^3)	27.0
	Young's modulus (MPa)	69.0
	Poisson's ratio	0.33

Table 2 Numerical parameters for DDA simulation in the small-scale model of the study site

Numerical parameters	Values
Maximum time increment (s)	0.001
Normal spring stiffness (kN/m)	380.0
Dynamic control parameter	0.99

5.3 Comparing the Results in the Experiment and DDA Simulation

Figure 6 shows the surface subsidence profiles obtained from the trap-door model and the DDA simulation. The X-axis shows the distance along with the trap-door panel (left-to-right). The black rectangle near the X-axis represents the location of the trap door. The Y-axis is the subsidence normal to the ground surface. The experimental ground-subsidence profile (solid line) correlates well with the DDA results (short-dashed line). The ground-subsidence profiles are asymmetric due to the inclined angle (α = 5°) of the mining. The maximum subsidence has a tendency to move to the right side of the trap-door, as clarified in research by Do *et al.* (2017). In addition, in Fig. 6, the shape effect of changing the aluminum rods in the trap-door tests to frictionless joints in DDA can be the main reason to cause the shape difference of ground settlement curves especially near the boundaries of the trap-door.

Figure 7 shows the normalized earth-pressure curves from the experimental and DDA results. The Y-axis shows normalization of earth-pressure in the direction perpendicular to the ground surface. The normalization of earth-pressure measured by the thirteen load cells in the experimental trap-door test is shown by solid triangles, and the corresponding DDA result is shown by the short-dashed line. Both the experimental and DDA results show significant stress concentration at the two trap-door boundaries as well as the asymmetry of the normalized earth-pressure curves. The stress concentration near the trap-door panel on the right side is higher than that on the left side, which explains the unbalanced shape of the trough subsidence (Fig. 6). In addition, the rock blocks near the right edge of the trap-door panel suffer very high stress during mining extraction, almost four times of increase of the initial earth stress. At the left corner of the trap-door in Fig. 7, the vertical stress from DDA is significantly lower than that from

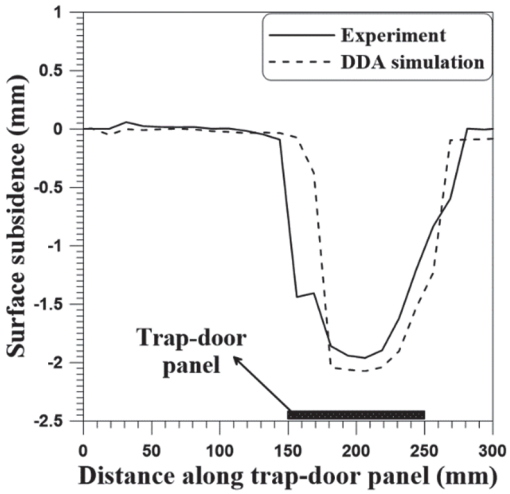

Fig. 6 Surface subsidence profiles of the small-scale model of the study site

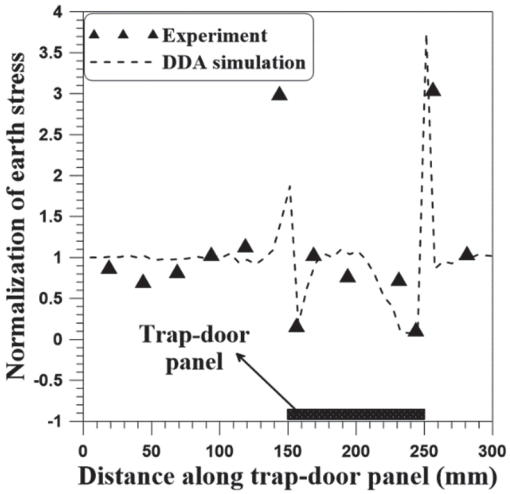

Fig. 7 Curves of normalization of earth pressure of the small-scale model of the study site

the trap-door tests. The rod packing at the left corner of the trap-door in the trap-door test can be the main reason to have the stress differences.

Figure 8 shows the movement of the blocks in the experiment and DDA simulation. Figure 8(a) shows the displacement of each block; while, Figure 8(b) shows the location of each block at the end of the simulation. The lowering trap-door panel induces downward movement of the blocks above the trap-door panel while the adjacent blocks are stationary. Figure 9 shows the principal-stress distribution and the significant concentration of stress near the right edge of the trap-door panel in the DDA simulation. Figures 7 and 9 imply that the high-stress concentration at the right edge of the trap-door panel may cause the rocks to fracture and fail due to mining extraction near the slope toe, thereby destabilizing the slope toe if the blocks in Zone A and the trap-door frame are removed (Fig. 9).

All in all, the stress concentration (Fig. 7) and the good correlation of the experimental trap-door test with the DDA simulation regarding surface subsidence (Fig. 6) verify the correctness of DDA to simulate the jointed rock mass movement from the mining of a tilted coal seam. Therefore, DDA is applied to reproduce the real geometry model of the coal mine at Nattai North of Australia. The mechanical behaviors of the rock cliff in the pre-landslide scenario are discussed through DDA simulation results.

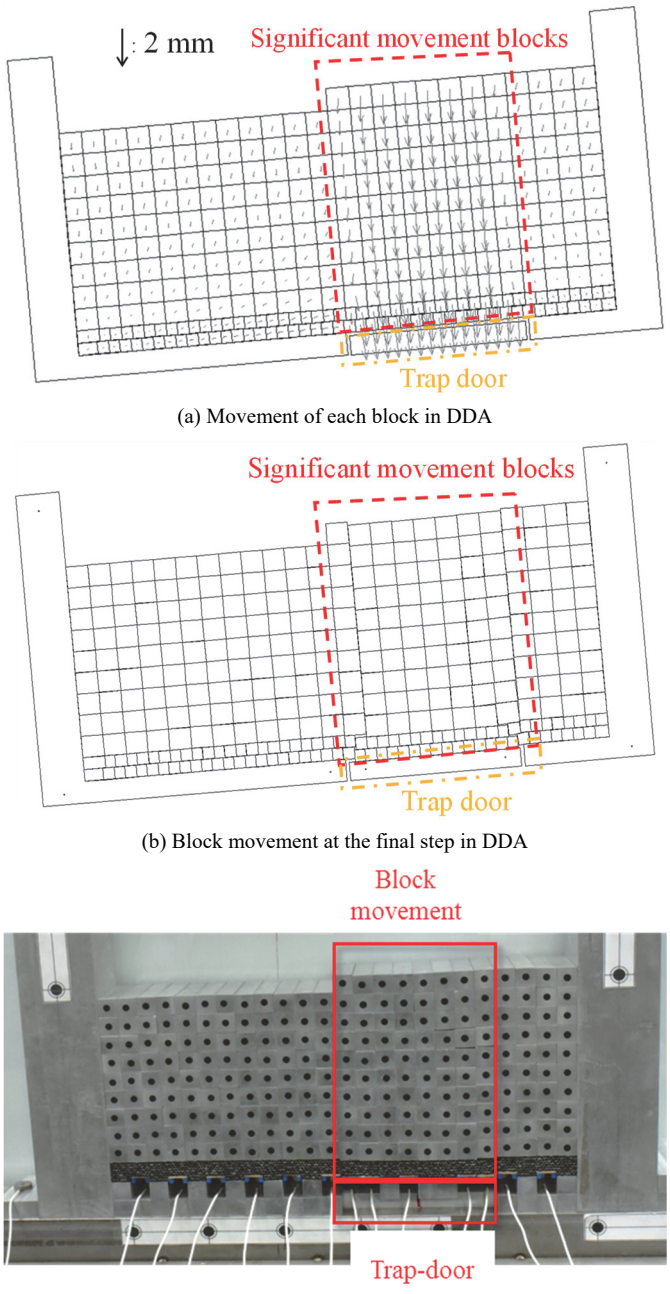

Fig. 8 Movements of blocks in the small-scale model of the study site

6. NEAR-SLOPE TILTED-SEAM MINING EXTRACTION IN NATTAI NORTH OF AUSTRALIA

6.1 Geometry Model of the Rock Slope at Nattai North of Australia in DDA Simulation

Figure 10 shows the geometry of the rock cliff in DDA based on the cross-section A-A' in Fig. 2. Table 3 shows the detailed information for creating a geometrical model of the rock slope at Nattai North of Australia (Mostyn *et al.* 1997). The rock mass consists of two sets of continuous discontinuities. The first set consists of the bedding planes of the rock masses tilting 5° into the slope. The second set consists of the near-vertical joints parallel to the

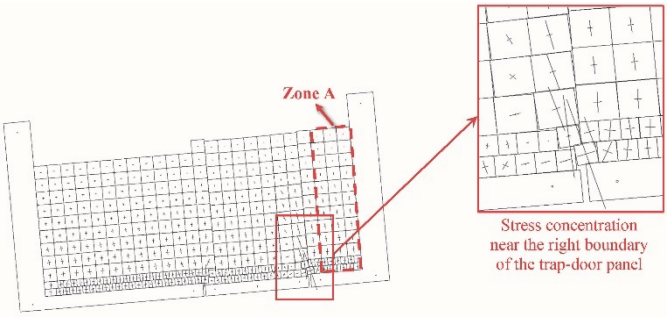

Fig. 9 Principal stress distribution in the small-scale model of the study site with DDA simulation

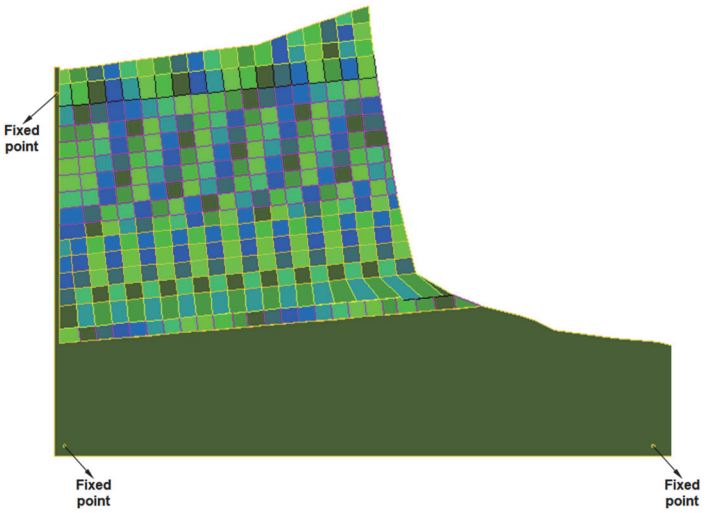

(a) The geometry model of the escarpment before mining operation

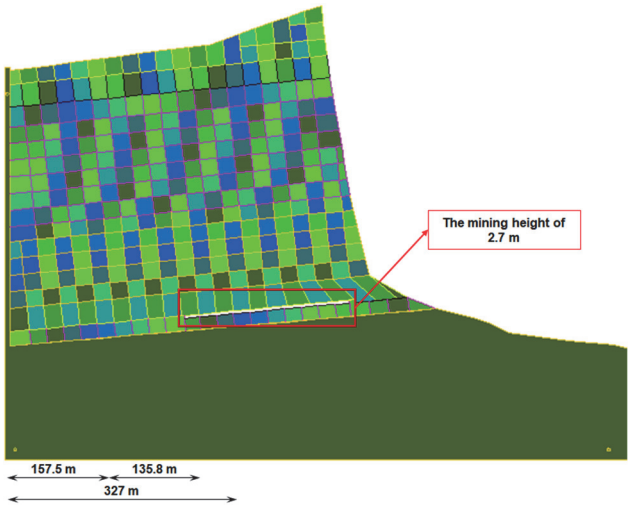

(b) The geometry model of the escarpment during mining operation

Fig. 10 The geometry model of the case study at Nattai North of Australia in DDA simulation

slope face (dip angle, 84°) (Fathi Salmi *et al.* 2017). The spacing of the bedding planes and of the vertical joints are equally set (14 m × 14 m), which avoids negative edge effects in the numerical simulation model (Mostyn *et al.* 1997). The base rock is fixed by the fixed points (Fig. 10(a)). The gap with dimension (2.7 m of height and 135.8 m of horizontal width) represents the coal mining in the Bulli seam layer (Fig. 10(b)). Table 4 summarizes the physical properties of the each geological strata in Fig. 2 and the characteristics of the discontinuities (Fathi Salmi *et al.* 2017) for DDA. Table 5 shows the numerical parameters that are used in the DDA simulation. Fully dynamic analysis will be carried out when the value of dynamic control parameter in Table 1 is set to be 1.0 because the dynamic post-failure simulation of the landslide.

6.2 Mechanical Behaviors of the Rock Slope in DDA Simulations

Figure 11 shows the distribution of the principal stress in the rock mass before and after the mining operations. Without the mining activity, the near-vertical stress from the gravity of the rock mass dominates the local principal stress (Fig. 11(a)). However, during mining excavation, stress is concentrated and an arching effect occurs in the vicinity of the mining zone (red line in Fig. 11(b)), especially near the toe of the slope. The phenomenon of stress concentration (Fig. 11(b)) similarly occurs in the small-scale model of the experimental trap-door test in Fig. 9.

Mining extraction causes movement of overlying rock strata into the created void and corresponding surface subsidence. The maximum surface subsidence is approximately 1.85 m (Fig. 12(a)). The earth pressure significantly increases (5.8 times near the slope toe) when the mining is excavated (Fig. 12(b)), which is similar with the phenomenon in the small-scale model of the study site in Fig. 7. Figure 13 shows the displacement of each block when the mining is excavated. The increase in both vertical and shear stress bends some blocks near the edge of the mining zone (Fig. 14). Surely, the displacement of each block provides quantitative value to assess the relative displacement along a joint. In this study, significant relative displacement along a joint is visually judged. Each

Table 3 Joint orientation and spacing for creating geometry model of rock cliff at Nattai North of Australia in DDA simulation referred from Mostyn *et al.* (1997)

Parameter	Applied to	Adopted parameters from Mostyn *et al.* (1997)	Model in DDA simulation
Dip angle (^{0})	vertical joints	84	84
	bedding discontinuities	–5*	–5*
Spacing (m)	vertical joints	14, 30, 125, 250	14
	bedding discontinuities	14, 30, 90, 180	14
Discontinuity persistence	all discontinuities	continuous	continuous

* The negative dip angle represents the joint dipping inward the slope

Table 4 Physical properties of the rock mass referred from Fathi Salmi *et al.* (2017)

	Hawkesbury sandstone	Bald Hill claystone	Bulgo sandstone	Scarborough sandstone	Wombarra claystone	Bulli seam	Bedrock
Friction angle (°)	34.0	28.0	32.0	32.0	28.0	26.0	33.0
Cohesion (kPa)	25.0	30.0	25.0	25.0	30.0	20.0	25.0
Tensile strength (kPa)	750.0	600.0	750.0	750.0	600.0	750.0	750.0
Density (g/cm^3)	2.397	2.719	2.527	2.514	2.643	1.5	2.569
Young's modulus (GPa)	14.0	10.4	18.0	20.6	17.0	2.8	18.2
Poisson's ratio	0.29	0.43	0.23	0.23	0.35	0.3	0.28

Table 5 Numerical parameters for DDA simulation of the case study at Nattai North of Australia

Numerical parameters	Values
Maximum time increment (s)	0.001
Normal spring stiffness (GPa/m)	1.0
Dynamic control parameter	1

joint is continuous at the beginning of the simulation. When two blocks have significant relative sliding movement along a joint, the non-parallel joints of the two blocks will be discontinuous. By following the definition, the red lines in Fig. 14 are the joints with significant shearing movements in the rock mass as cracking. The cracks above the mining zone extend to the ground surface (Fig. 14).

DDA successfully simulates the ground movement and the stress concentration of the jointed rock mass subjected to tilted-seam mining extraction in the small-scale model of the study site (Figs. 6 to 9) as well as the case study of Nattai North coal mine (Figs. 11 to 14). Therefore, the failure mechanisms at this coal mine can be concluded as that the inward-tilting seam generates unsymmetrical stress concentration near the two sidewalls of the mining. Higher stress concentration occurs at the side nearer the slope surface than at the site away from the slope surface (Fig. 12(b)).

Surprise, the landslide do not occur at the end of the DDA simulations in Fig. 12(b). The assumption of the elastic and unbreakable blocks could cause the inconsistence of DDA to the actual situation of Nattai north landslide. In this study, failure criteria are not added to the DDA code to generate block fracturing. Therefore, cracks are added artificially to the blocks near the slope face with large principal stresses by following Byerlee (1968) that the angle between the fracture and the maximum principal stress is

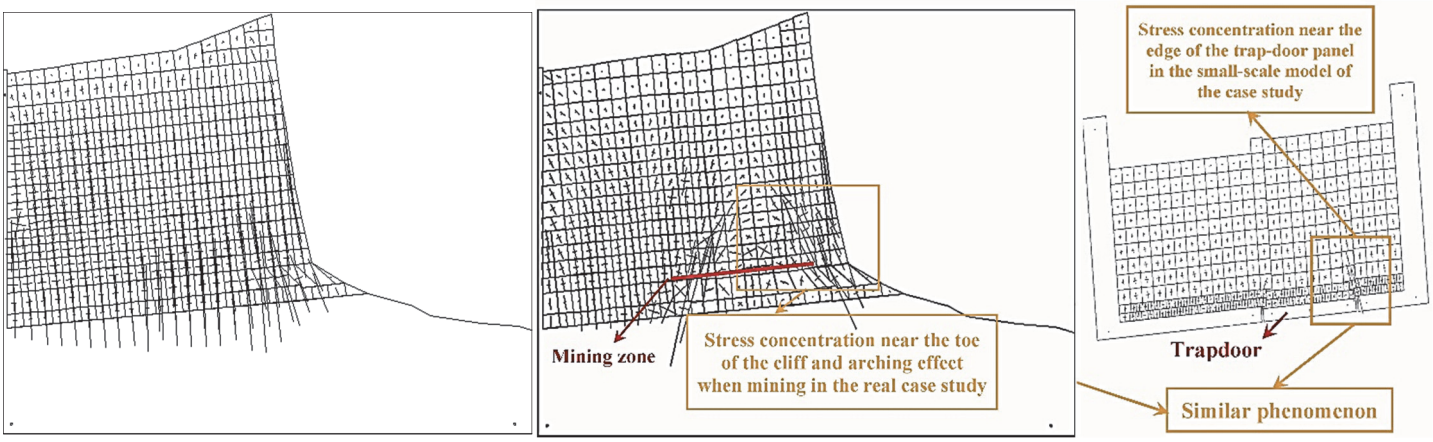

(a) Stress distribution of the escarpment before mining extraction

(b) Stress distribution of the escarpment during mining extraction showing the relationship between the stresσσ concentration in the case study and that in the small scale model of the case study

Fig. 11 Principal stress distribution around the mining zone in DDA simulation

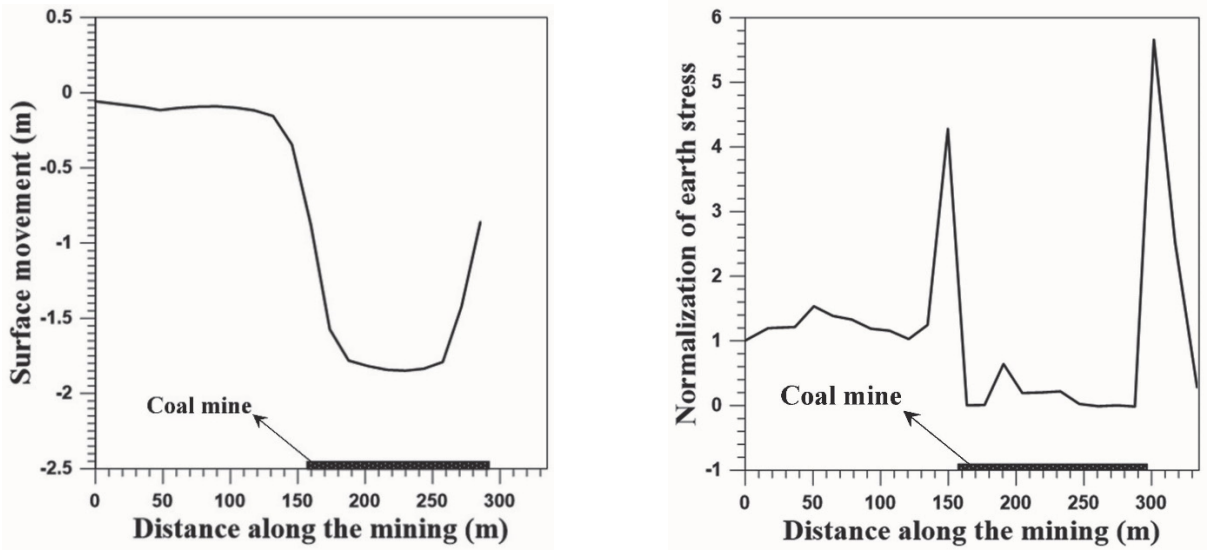

(a) Surface subsidence pattern

(b) Normalization of the earth pressure

Fig. 12 Surface subsidence and normalization of the earth stress in DDA simulation

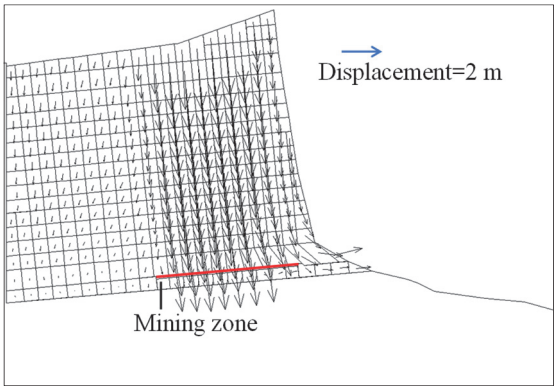

Fig. 13 Block displacement when mining extraction

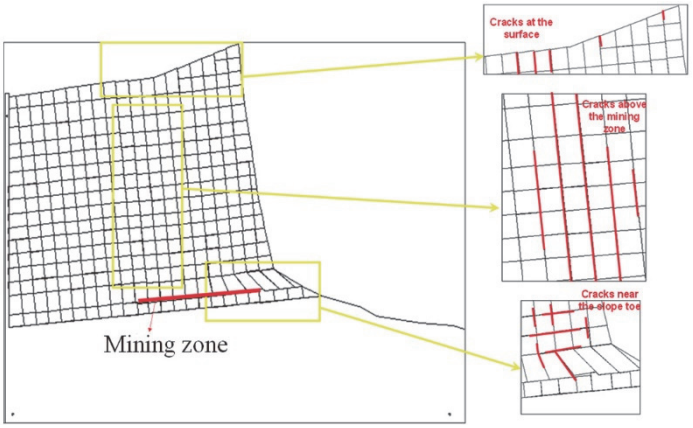

Fig. 14 Cracks appear when mining extraction

approximately 30° under uniaxial compression because the significant lateral stress release of rocks near the slope cliff approximates the rocks to the uniaxial compression. The DDA simulation results (Fig. 11(b)) show that the rock blocks near the slope toe at Wombarra Claystone and Scarborough Sandstone (Fig. 2) are subjected the maximum vertical stress, 16.26 MPa and 22.92 MPa respectively. While the uniaxial compressive strength of the rock blocks at the two strata is, 5.6 MPa and 19.4 MPa respectively (Fathi Salmi *et al.* 2017). The very high vertical stress may crack rock blocks near the slope toe at Wombarra Claystone and Scarborough Sandstone. In addition, the insufficient distance between the slope surface and the mining under concentrated stress may result in the rock mass to fracture and even fail at the slope toe and triggers the subsequent landslide. Therefore, Figure 15 shows that fractures are explicitly added to the blocks at the right stress arching with large principal stresses in Fig. 11(b) near the toe at Wombarra Claystone and Scarborough Sandstone in Fig. 2 in DDA. Figure 16 shows the post-failure simulations of kinematic movement of the Nattai North landslide using DDA.

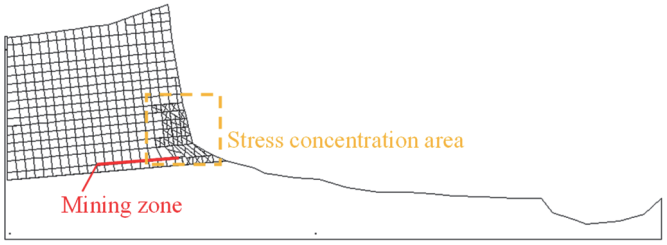

Fig. 15 Geometry of Nattai north landslide slope with fracturing in the stress concentration area

7. CONCLUSIONS

In this study, the DDA computational results correlate well with the experimental results from the trap-door model, which verifies the correctness of using DDA to simulate rock-mass behavior resulting from underground mining.

This study demonstrates that the block failure resulting from the high stress concentration near the toe of the slope and the edge of the mining zone induced the Nattai North landslide. DDA successfully simulates not only the shear displacements along joints but also the kinematic movement of the mining-induced landslide at the coal mine of Nattai North, Australia.

(a) 3.224 sec

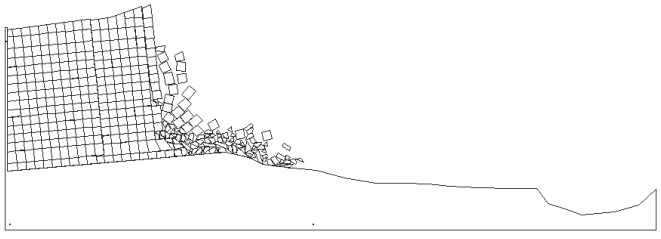

(b) 10.388 sec

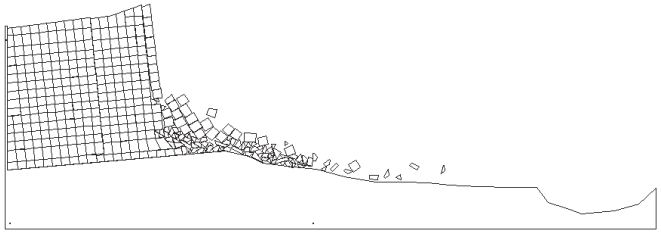

(c) 16.937 sec

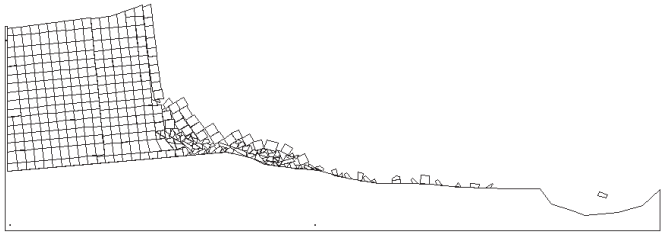

(d) 45.317 sec

Fig. 16 Post-failure simulation of the Nattai North landslide slope

ACKNOWLEDGMENTS

The authors would like to thank the kind assistance of all lab mates in Rock Laboratory at the Civil Engineering Department, National Cheng Kung University, Tainan, Taiwan.

FUNDING

Special thanks will give to the Ministry of Science and Technology, Taiwan for its financial support (Grant Number: MOST 105-2628-E-006 -004 -MY3) in this study.

DATA AVAILABILITY

The data in this study are available from the corresponding author on reasonable request.

CONFLICT OF INTEREST STATEMENT

The authors declare that there is no conflict of interest.

REFERENCES

Aleshina, I.N., Snytko, V.A., and Szczypek, S. (2008). "Mining-induced ground subsidences as the relief-forming factor on the territory of the Silesian Upland (Southern Poland)." *Geography and Natural Resources*, **29**(3), 288-291. https://doi.org/10.1016/j.gnr.2008.09.015

Ambrožič, T. and Turk, G. (2003). "Prediction of subsidence due to underground mining by artificial neural networks." *Computers & Geosciences*, **29**(5), 627-637. https://doi.org/10.1016/S0098-3004(03)00044-X

Bell, F.G., Stacey, T.R., and Genske, D.D. (2000). "Mining subsidence and its effect on the environment: some differing examples." *Environmental Geology*, **40**(1-2), 135-152. https://doi.org/10.1007/s002540000140

Bi, Y., Zhang, J., Song, Z., Wang, Z., Qiu, L., Hu, J., and Gong, Y. (2019). "Arbuscular mycorrhizal fungi alleviate root damage stress induced by simulated coal mining subsidence ground fissures." *Science of The Total Environment*, **652**, 398-405. https://doi.org/10.1016/j.scitotenv.2018.10.249

Britain, G. (1966). *Subsidence Engineers' Handbook*. National Coal Board, UK.

Carnec, C. and Delacourt, C. (2000). "Three years of mining subsidence monitored by SAR interferometry, near Gardanne, France." *Journal of Applied Geophysics*, **43**(1), 43-54. https://doi.org/10.1016/S0926-9851(99)00032-4

Castañeda, C., Gutiérrez, F., Manunta, M., and Galve, J.P. (2009). "DInSAR measurements of ground deformation by sinkholes, mining subsidence, and landslides, Ebro River, Spain." *Earth Surface Processes and Landforms*, **34**(11), 1562-1574. https://doi.org/10.1002/esp.1848

Chen, G., Wang, X., Wang, R., and Liu, G. (2019). "Health risk assessment of potentially harmful elements in subsidence water bodies using a Monte Carlo approach: An example from the Huainan coal mining area, China." *Ecotoxicology and Environmental Safety*, **171**, 737-745. https://doi.org/10.1016/j.ecoenv.2018.12.101

Chen, S.H., Wang, W., Zheng, H.F., Shahrour, I. (2010). "Block element method for the seismic stability of rock slopes." *Journal of Geotechnical and Geoenvironmental Engineering*, ASCE, **136**(12), 1610-1617. https://doi.org/10.1061/(ASCE)GT.1943-5606.0000391

Choi, J.K., Kim, K-D, Lee S., and Won J.S. (2010). "Application of a fuzzy operator to susceptibility estimations of coal mine subsidence in Taebaek City, Korea." *Environmental Earth Sciences*, **59**(5), 1009-1022. https://doi.org/10.1007/s12665-009-0093-6

Cunningham, D.M. (1988). "A rockfall avalanche in a sandstone landscape, Nattai North, NSW." *Australian Geographer*, **19**(2), 221-229. https://doi.org/10.1080/00049188808702961

Dai, H.Y., Ren, L.Y., Wang, M., and Xue, H.B. (2011). "Water distribution extracted from mining subsidence area using Kriging interpolation algorithm." *Transactions of Nonferrous Metals Society of China*, **21**, s723-s726. https://doi.org/10.1016/S1003-6326(12)61669-0

Do, T.N., Wu, J.H., and Lin, H.M. (2017). "Investigation of sloped surface subsidence during inclined seam extraction in a jointed rock mass using discontinuous deformation analysis." *International Journal of Geomechanics*, ASCE, **17**(8), 04017021. https://doi.org/10.1061/(ASCE)GM.1943-5622.0000894

Do, T.N. and Wu, J.H. (2020a). "Verifying discontinuous deformation analysis simulations of the jointed rock mass behavior of shallow twin mountain tunnels." *International Journal of Rock Mechanics and Mining Sciences*, **130**, 104322. https://doi.org/10.1016/j.ijrmms.2020.104322

Do, T.N. and Wu, J.H. (2020b). "Simulation of the inclined jointed rock mass behaviors in a mountain excavation using DDA." *Computers and Geotechnics*, **117**, 103249. https://doi.org/10.1016/j.compgeo.2019.103249

Dunrud, C.R. and Osterwald, F.W. (1980). *Effects of Coal Mine Subsidence in the Sheridan, Wyoming, Area*. United States Geological Survey Professional Paper 1164, USA.

Fathi Salmi, E., Nazem, M., and Karakus, M. (2017). "Numerical analysis of a large landslide induced by coal mining subsidence." *Engineering Geology*, **217**, 141-152. https://doi.org/10.1016/j.enggeo.2016.12.021

Ghabraie, B., Ren, G., Zhang, X., and Smith, J. (2015). "Physical modelling of subsidence from sequential extraction of partially overlapping longwall panels and study of substrata movement characteristics." *International Journal of Coal Geology*, **140**, 71-83. https://doi.org/10.1016/j.coal.2015.01.004

Holla, L. (1997). "Ground movement due to longwall mining in high relief areas in New South Wales, Australia." *International Journal of Rock Mechanics and Mining Sciences*, **34**(5), 775-787. https://doi.org/10.1016/S1365-1609(97)00004-1

Jing, L., Ma, Y., and Fang, Z. (2001). "Modeling of fluid flow and solid deformation for fractured rocks with discontinuous deformation analysis (DDA) method." *International Journal of Rock Mechanics and Mining Sciences*, **38**(3), 343-355. http://dx.doi.org/10.1016/S1365-1609(01)00005-3

Jing, Z., Wang, J., Zhu, Y., and Feng, Y. (2018). "Effects of land subsidence resulted from coal mining on soil nutrient distributions in a loess area of China." *Journal of Cleaner Production*, **177**, 350-361. https://doi.org/10.1016/j.jclepro.2017.12.191

Keilich, W., Seedsman, R.W., and Aziz, N. (2006). "Numerical modelling of mining induced subsidence." in Naj Aziz and Bob Kininmonth, Eds., *Proceedings of the 2006 Coal Operators' Conference, Mining Engineering*, University of Wollongong, 18-20

Meguid, M.A., Saada, O., Nunes, M.A., and Mattar, J. (2008). "Physical modeling of tunnels in soft ground: A review." *Tunnelling and Underground Space Technology*, **23**(2), 185-

198. http://dx.doi.org/10.1016/j.tust.2007.02.003

Mostyn, G., Helgstedt, M.D., and Douglas, K.J. (1997). "Towards field bounds on rock mass failure criteria." *International Journal of Rock Mechanics and Mining Sciences*, **34**(3), 208.e1-208.e18. https://doi.org/10.1016/S1365-1609(97)00163-9

Najjar, Y. and Zaman, M. (1993). "Numerical modeling of ground subsidence due to mining." *International Journal of Rock Mechanics and Mining Sciences & Geomechanics Abstracts*, **30**(7), 1445-1448. https://doi.org/10.1016/0148-9062(93)90135-Z

Park, SH. (2001). *Mechanical Behavior of Ground with Inclined Layers during Tunnel Excavation*. Ph.D. Dissertation, School of Civil Engineering, Kyoto University, Japan.

Park, S.H. and Adachi, T. (2002). "Laboratory model tests and FE analyses on tunneling in the unconsolidated ground with inclined layers." *Tunnelling and Underground Space Technology*, **17**(2), 181-193. http://dx.doi.org/10.1016/S0886-7798(02)00003-2

Pells, PJN, Braybrooke, JC, and Mong, J. (1987). "Cliff line collapse associated with mining activities." in Walker, B.F. and Fell, R., Eds., *Slope Instability and Stabilization*, Balkema, Rotterdam, 359-385.

Sasaoka, T., Takamoto, H., Shimada, H., Oya, J., Hamanaka, A., and Matsui, K. (2015). "Surface subsidence due to underground mining operation under weak geological condition in Indonesia." *Journal of Rock Mechanics and Geotechnical Engineering*, **7**(3), 337-344. https://doi.org/10.1016/j.jrmge.2015.01.007

Shi, G.H. and Goodman, R.E. (1989). "Generalization of two-dimensional discontinuous deformation analysis for forward modelling." *International Journal for Numerical and Analytical Methods in Geomechanics*, **13**(4), 359-380. https://doi.org/10.1002/nag.1610130403

Singh, R.P. and Yadav, R.N. (1995). "Prediction of subsidence due to coal mining in Raniganj coalfield, West Bengal, India." *Engineering Geology*, **39**(1), 103-111. https://doi.org/10.1016/0013-7952(94)00062-7

Song, J., Han, C., Li, P., Zhang, J., Liu, D., Jiang, M., Zheng, L., Zhang, J., and Song, J. (2012). "Quantitative prediction of mining subsidence and its impact on the environment." *International Journal of Mining Science and Technology*, **22**(1), 69-73. https://doi.org/10.1016/j.ijmst.2011.07.008

Tanaka, T. and Sakai, T. (1993). "Progressive failure and scale effect of trap-door problems with granular materials." *Soils and Foundations*, **33**(1), 11-22. https://doi.org/10.3208/sandf1972.33.11

Thongprapha, T., Fuenkajorn, K., and Daemen, J.J.K. (2015). "Study of surface subsidence above an underground opening using a trap door apparatus." *Tunnelling and Underground Space Technology*, **46**, 94-103. https://doi.org/10.1016/j.tust.2014.11.007

Vyazmensky, A., Elmo, D., Stead, D., and Rance, J.R. (2007). "Combined finite-discrete element modelling of surface subsidence associated with block caving mining." In *Rock Mechanics: Meeting Society's Challenges and Demands*, Two Volume Set, 467-475. Taylor & Francis.

Wu, J.H. (2010). "Compatible algorithm for integrations on a block domain of any shape for three-dimensional discontinuous deformation analysis." *Computers and Geotechnics*, **37**(1-2), 153-163. https://doi.org/10.1016/j.compgeo.2009.08.009

Wu, J.H. and Hsieh, P.H. (2021a). "Numerical assessment of the impact area and the geometry of a landslide dam: the Nan-Shi-Keng landslide, Taiwan." *Journal of GeoEngineering*, **16**(4), 155-167. https://doi.org/10.6310/jog.202112_16(4).4

Wu, J.H. and Hsieh, P.H. (2021b). "Simulating the postfailure behavior of the seismically-triggered Chiu-fen-erh-shan." *Engineering Geology*, **287**, 106113. https://doi.org/10.1016/j.enggeo.2021.106113

Wu, J.H., Ohnishi, Y., and Nishiyama, S. (2004). "Simulation of the mechanical behavior of inclined jointed rock masses during tunnel construction using Discontinuous Deformation Analysis (DDA)." *International Journal of Rock Mechanics and Mining Sciences*, **41**(5), 731-743. http://dx.doi.org/10.1016/j.ijrmms.2004.01.010

Wu, W., Zhu, H., Lin, J.S., Zhuang, X., and Ma, G. (2018). "Tunnel stability assessment by 3D DDA-key block analysis." *Tunnelling and Underground Space Technology*, **71**, 210-214. https://doi.org/10.1016/j.tust.2017.07.015

Xu, N., Kulatilake, P.H.S.W., Tian, H., Wu, X., Nan, Y., and Tian, W. (2013). "Surface subsidence prediction for the WUTONG mine using a 3-D finite difference method." *Computers and Geotechnics*, **48**, 134-145.

Yang, X. and Ho, P. (2019). "Is mining harmful or beneficial? A survey of local community perspectives in China." *The Extractive Industries and Society*, **6**(2), 584-491. https://doi.org/10.1016/j.exis.2019.02.006

Zheng, L., Liu, X., Tang, Q., and Ou, J. (2019). "Lead pollution and isotope tracing of surface sediments in the huainan panji coal mining subsidence area, Anhui, China." *Bulletin of Environmental Contamination and Toxicology*, **103**, 10-15. https://doi.org/10.1007/s00128-019-02558-5

Zhu, H., Wu, W., Chen, J., Ma, G., Liu, X., and Zhuang, X. (2016). "Integration of three dimensional discontinuous deformation analysis (DDA) with binocular photogrammetry for stability analysis of tunnels in blocky rockmass." *Tunnelling and Underground Space Technology*, **51**, 30-40. https://doi.org/10.1016/j.tust.2015.10.012